Scripta Materialia 271 (2026) 116983

Contents lists available at ScienceDirect

Scripta Materialia

journal homepage: www.journals.elsevier.com/scripta-materialia

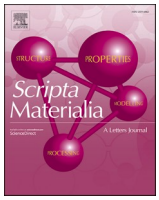

Thermodynamic modeling and experimental study of protective barriers against carbon diffusion during spark plasma sintering process

R. Charvet [a,*], M.R. Ardigo-Besnard [a], A. Besnard [b], F. Baras [a], S. Le Gallet [a], Y. Pinot [c], F. Herbst [a], F. Bernard [a]

[a] Université Bourgogne Europe, CNRS, Laboratoire Interdisciplinaire Carnot de Bourgogne ICB UMR 6303, F-21000 Dijon, France
[b] Université Marie et Louis Pasteur, SUPMICROTECH, CNRS, Institut FEMTO-ST, F-25000, Besançon, France
[c] Arts et Metiers Institute of Technology, LaBoMaP, 71250 Cluny, France

ARTICLE INFO

Keywords:
Spark plasma sintering
CALPHAD
Carbon diffusion
Thermodynamics
Physical vapor deposition (PVD)

ABSTRACT

During spark plasma sintering (SPS), the contact between the graphite tooling and the powder results in carbon diffusion. Graphite foils coated with a physical vapor deposition (PVD) film represent a promising solution to overcome this issue. In the present work, simulation and experiments were combined to understand the barrier effectiveness against carbon diffusion of a titanium PVD film deposited on graphite foils used during SPS of an iron powder. In non-equilibrium processes, simulation alone is insufficient to describe the multiple diffusion scenarios. On the other hand, experimental measurements are not always relevant. The approach adopted in this work enabled the prediction of the potential phases that form as a function of diffusion depth. Several scenarios were proposed, helping to explain the influence of the film thickness. This methodology, applied to the C-Ti-Fe system, can be extended to other film-substrate couples, reducing the number of tests and the associated costs.

The improvement of the durability properties of metal parts is a major issue for many industrial sectors, such as aeronautics, aerospace, military, etc. A fine and homogeneous microstructure is usually sought, leading to improved mechanical properties [1,2]. The elaboration of metallic parts by powder metallurgy techniques, such as spark plasma sintering (SPS), represents an alternative way to conventional manufacturing methods (*i.e.*, casting, forging, or machining) [3]. During SPS, the powder is densified through the simultaneous application of heating (by Joule effect via a direct or pulsed current) and pressure (via a uniaxial load). This fast sintering limits grain growth [4]. SPS enables the elaboration, in a single step, of high-performance materials with controlled chemical compositions [5] and enhanced mechanical properties [6]. SPS requires the use of graphite tooling (punches and dies), and graphite foils are inserted between the powder and the surfaces in contact with the tooling. This ensures good electrical, physical, and thermal contact of the tooling-powder assembly and facilitates demolding. Therefore, in the case of metallic powders, carbon diffusion from graphite leads to the formation of secondary undesirable phases (generally carbides) at the surface of the sintered sample. Moreover, carbon diffusion towards the bulk occurs and leads to the degradation of the properties of the sintered materials [7].

An existing solution to prevent carbon diffusion is spraying boron nitride (BN) on the graphite foils. However, BN is an electrical insulator and can be damaged during compaction and densification, when the powder and the punch move relative to the die [8]. The homogeneity of the sprayed layer is not guaranteed, and components of the BN powder or the silicon-based adhesive can contaminate the sintered material. Another solution consists of inserting a metal foil of a carbide-forming element between the powder and the graphite foil [9]. However, this strategy does not represent a large-scale solution and is difficult to apply to sintered parts with complex shapes. Recently, the use of graphite foils coated with a physical vapor deposition (PVD) film gave promising results [10]. The main advantage of this approach is that PVD provides precise control over film thickness and ensures uniform coverage of surfaces, including complex shapes [11], making it well-suited for industrial-scale applications. Graphite foils coated by a Ti PVD film of at least 1.1 μm thickness were effective in preventing carbon diffusion during the sintering of Fe, while a thickness of 0.5 μm was not sufficient to ensure full protection [10]. The influence of the thickness of a film on the diffusion of light elements has also been reported in the Ti-Al-O system [12]. In the present study, by coupling diffusion simulations and SPS experiments, the impact of titanium film thickness on its

* Corresponding author.
E-mail address: romain.charvet@ube.fr (R. Charvet).

https://doi.org/10.1016/j.scriptamat.2025.116983
Received 20 May 2025; Received in revised form 29 July 2025; Accepted 3 September 2025
Available online 8 September 2025

protective behavior against carbon diffusion during SPS of an iron powder was explored. The approach adopted in this work allows the prediction of potential phases formed during a non-equilibrium process as a function of diffusion depth, thus enabling the understanding and explanation of the influence of film thickness. This approach can be transposed to other film-substrate systems, advancing the development of cost-effective and large-scale solutions to limit carbon diffusion during SPS.

Titanium films were deposited on graphite foils using a PVD system KS40V (Kenosistec, Binasco, Italy), equipped with a Ti target (99.95 at. % purity, 406 × 120 × 6 mm). The sample holders were placed on a carousel (550 mm diameter, 90 mm minimal target-to-substrate distance) rotating at 0.7 rpm, with a flow of 80 sccm of argon, a working pressure of 0.45 Pa, and a power of 1500 W (4.4 A, 340 V). Titanium film thicknesses of 0.6, 0.9, and 1.2 μm were obtained for deposition durations of 87, 130, and 160 min, respectively. Iron powder (99.7 at. % purity), supplied by Höganäs (Sweden), presents a granulometry ranging from 50 to 200 μm. The particles exhibit an irregular morphology (supplementary material S1), typical of water atomization. Two kinds of samples were sintered by SPS, using uncoated (reference sample) and Ti-coated graphite foils. The SPS cycle consisted of a 50 °C/min heating ramp up to 1050 °C, followed by a dwell of 10 min at 1050 °C under an applied pressure of 70 MPa, and a natural cooling.

Characterizations were performed on the samples' cross-sections. Sintered disks (30 mm diameter, 5 mm height) were cut along the axial direction, and the cross-section surfaces were then polished using SiC papers (down to 1200 grit), diamond suspensions (down to 1 μm), and colloidal silica (0.03 μm). Microstructural observations were performed after Nital etching (3 %, 15 s), using an optical microscope (AXIO, Zeiss, Germany). The carburization phenomenon was investigated by cross-sectional wavelength dispersive X-ray spectrometer (WDX) profiles, by using a JSM-7610F scanning electron microscope (SEM) (Jeol, Japan) with an accelerating voltage of 5 kV. The carbon concentration was calculated based on the number of hits per μA, using a calibration curve obtained under the same conditions with reference samples. For each sample, three profiles were measured, giving an average measurement uncertainty of 0.12 wt. %. Energy Dispersive X-ray spectroscopy (EDX) measurements were carried out to investigate Ti-Fe interdiffusion phenomena. At 5 kV, the radius of the analyzed area was around 90 nm.

Thermodynamic diffusion simulations were performed using the Thermo-Calc® DICTRA module, with the TCFE12 and MOBFE7 databases. The boundary condition of an infinite carbon source (activity equal to 1, graphite as reference state) in $x = 0$ was assumed (supplementary material S2). The simulation temperature was set to 1000 °C, based on experimental measurements close to the sample, and for 10 min, corresponding to the dwell time. An isopleth section at 1000 °C of the Ti-C-Fe ternary phase diagram was also calculated to investigate the stable phases present at specific chemical compositions.

The microstructure of the sample sintered with uncoated graphite foils was consistent with that observed in a previous study [10]. Four zones with decreasing carbon concentration can be distinguished, from the graphite foil/sintered powder interface to the bulk (Fig. 1(a)):

- a hyper-eutectoid area, composed of pro-eutectoid cementite (Fe_3C), surrounded by a layer of abnormal ferrite, and pearlite (Fig. 1(b));
- an eutectoid area composed of sole pearlite (Fig. 1(c));
- a hypo-eutectoid area with pearlite and ferrite (Fig. 1(d));
- the ferritic matrix unaffected by carbon diffusion (Fig. 1(e)).

The carbon diffusion profiles of the SPS samples sintered with graphite foils coated by titanium films of three different thicknesses are summarized in Fig. 2. An optical microscope cross-section image of the sample sintered using uncoated graphite foils is added for comparison and correlated with the corresponding WDX carbon profile. The agreement between the four zones previously identified in Fig. 1 and the measured carbon concentration profile is good. Indeed, carbon concentration ranges between 2 and 1.2 wt. % in the hypereutectoid zone (depth between 0 and 180 μm). Carbon content is between 1.2 and 0.6 wt. % in the eutectoid area (depth between 180 and 350 μm), with the center being around 0.8 wt. % (depth of 250 μm), as expected for a eutectoid composition. Finally, the carbon value is between 0.6 and 0.1 wt. % in the hypoeutectoid region (depth between 350 and 610 μm) and is almost equal to zero in the iron matrix (depth higher than 610 μm).

For the sample sintered using graphite foil coated with a 0.6 μm-thick titanium film, the carbon concentration profile is lowered compared to the reference sample. Optical microscopy observations revealed the presence of eutectoid and hypoeutectoid zones (supplementary material S3 (a)), indicating that carbon diffusion was not hindered. For the sample sintered with graphite foil coated with a 0.9 μm-thick titanium film, carbon diffusion is reduced. Only the hypoeutectoid area is observable (supplementary material S3 (b)). When the sample is

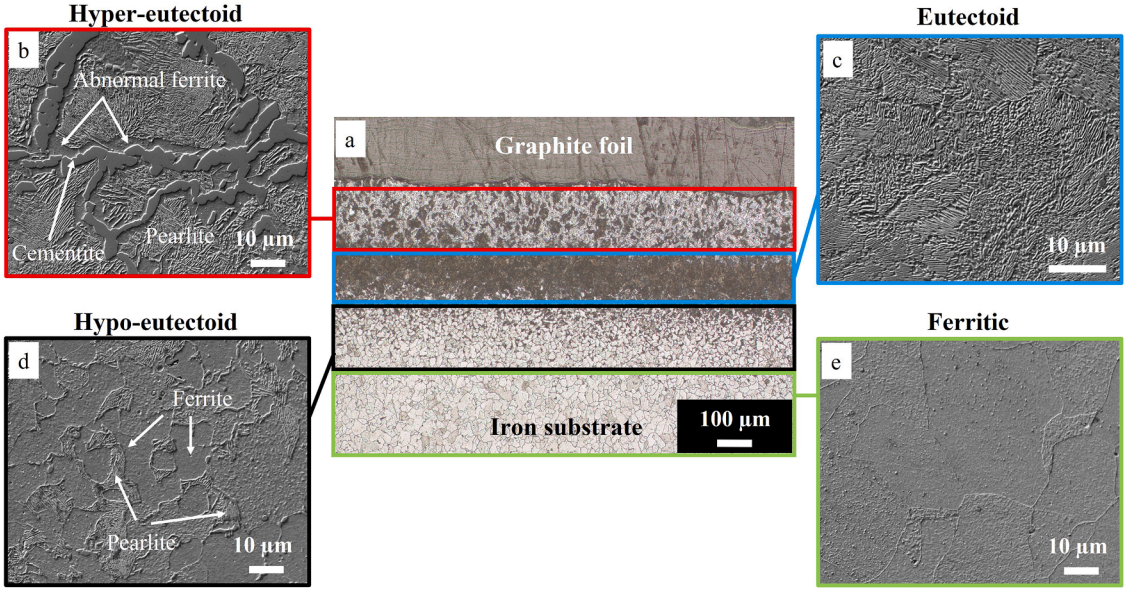

Fig. 1. Sample sintered with uncoated graphite foils: (a) optical micrography after chemical etching, and (b-e) SEM images of the different zones.

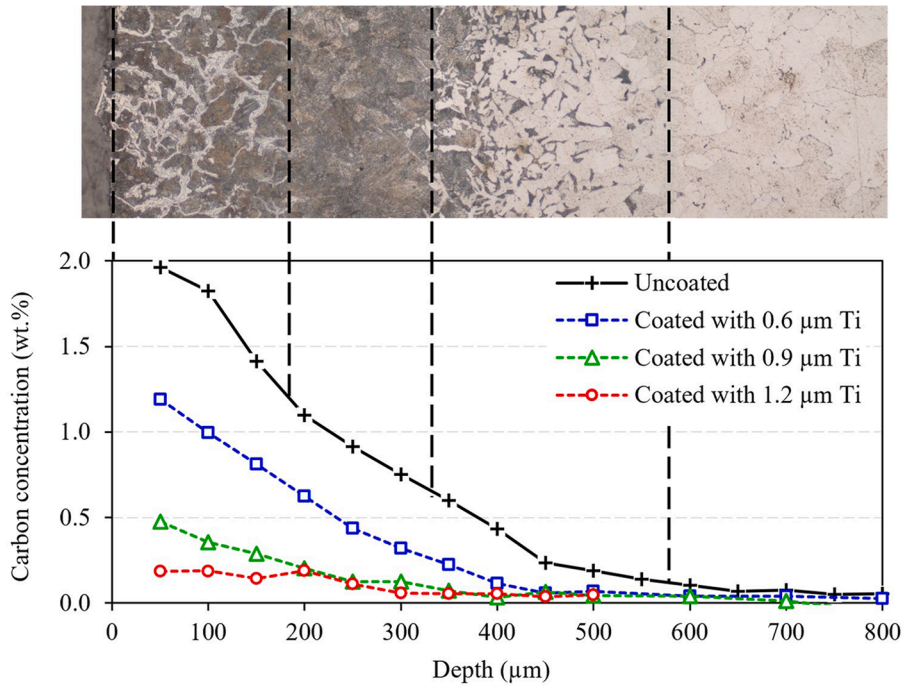

Fig. 2. Carbon WDX profiles of the samples sintered with uncoated graphite foil and with graphite foils coated with a PVD titanium film of 0.6, 0.9, and 1.2 μm. The optical micrograph represents the uncoated sample.

sintered with graphite foil coated with a 1.2 μm-thick titanium film, carbon diffusion is almost completely blocked, in agreement with microstructural observations (supplementary material S3 (c)). Residual carbon contamination (approximately 0.1 wt. % at a depth of up to 250 μm from the interface) is present and may be explained by local growth heterogeneities of the film, which are neglected in thermodynamic simulations.

To understand the barrier effectiveness of the film against carbon diffusion, the diffusion of the species (carbon and iron) in the titanium film must be investigated. Two limit cases can be identified: diffusion of carbon exclusively in titanium, corresponding to carbon diffusion from one side of the titanium film, and diffusion of iron exclusively in titanium, corresponding to iron diffusion from the opposite side of the titanium film. The diffusion of carbon in titanium was simulated with Thermo-Calc® DICTRA (Model A) (supplementary material S2). This system consists of carbon in contact with 2 μm of pure titanium. Fig. 3(a) shows the carbon profile after 10 min. Simulation results of model A predict carbon diffusion in the titanium film up to about 1.1 μm depth. According to the Ti-C phase diagram, the carbon concentration (15.3 wt. %) at the interface corresponds to the TiC phase. The carbon concentration of 12.3 wt. % observed until a depth of 0.5 μm corresponds to the minimum carbon content of the TiC domain. Beyond this depth, a mixture of Ti and TiC is present, with a decreasing proportion. This observation aligns with a previous study, which demonstrated that the application of a 1.1 μm titanium film is effective in completely preventing the carburization of pure iron powder, if only carbon diffuses [10]. However, it is known from the Fe-Ti binary diagram, and it is well documented in the literature [13], that Fe-Ti interdiffusion occurs at high temperature, leading to FeTi and Fe_2Ti intermetallic compounds formation in addition to Fe(Ti) and Ti(Fe) solid solutions. Fig. 3(b) presents the experimentally measured interdiffusion of Ti and Fe during sintering with a 1.2 μm-thick titanium film (Model B). Fe reaches a depth of 0.3 μm, the stoichiometry of the FeTi phase is found around 0.5 μm, and the stoichiometry of the Fe_2Ti phase is present on a small length of 0.1 μm around a depth of 0.7 μm.

In the real system, simultaneous carbon and iron diffusion in the titanium film occurs from the opposite sides of the film. However, simulating the homogenization of the C-Ti-Fe system was extremely difficult and slow, and it was not possible to significantly increase the simulation speed and to obtain meaningful results. Due to the very low carbon solubility into titanium (0.15 wt. % at 1000 °C), it was assumed that the TiC phase forms almost immediately as carbon starts to diffuse, justifying the use of the C-TiC-Fe simulation model as a first approach and third limit case. This diffusion of carbon and iron into TiC was investigated with Thermo-Calc® DICTRA (Model C) (supplementary material S2). This system consists of carbon in contact with 1 μm of titanium carbide and 4 μm of iron. Fig. 3(c) shows the carbon profile after 10 min. Simulation indicates that iron diffusion also occurs in the ternary C-TiC-Fe system, reaching a depth of 0.5 μm. Whatever the amount of iron that diffuses into the TiC, only a mixture of α-Fe and TiC phases is present, in different proportions along the depth. A small amount (2 wt. %) of titanium also diffuses into the iron over a distance of 9 μm.

However, under real sintering conditions, carbon and iron diffuse simultaneously from both sides into the titanium film, rather than into TiC as assumed in model C. The C-Ti-Fe isopleth section at 1000 °C helps predict the phases likely to form under real conditions, depending on the carbon concentration at different penetration depths. Five representative scenarios were examined based on the phase equilibria observed in the isopleth at this temperature (Fig. 4). The experimental EDX measurements of Fe and Ti served as a basis and were adjusted using the theoretical carbon content estimated to remain within the assumed phase domain.

In all scenarios, TiC is presumed to form at the C-Ti interface and will then coexist, in decreasing fraction, with the different Ti-Fe phases throughout the film depth. In scenario 1, based on model C, TiC coexists with α-Fe. In this scenario, when the film-Fe interface is reached at a depth of 1 μm, carbon is combined with titanium to form TiC, and carbon content dissolved in α-Fe is 0 wt. %. In scenario 2, Fe_2Ti is present. In scenario 3, TiFe forms, while in scenario 4, Fe is in solid solution in β-Ti. In these three scenarios, when the film-Fe interface is reached at a depth of 1 μm, the carbon content is equal to zero. In the first four scenarios, the barrier effect of the film is guaranteed, and the iron is not contaminated by carbon. In scenario 5, TiC coexists with α-Fe near the

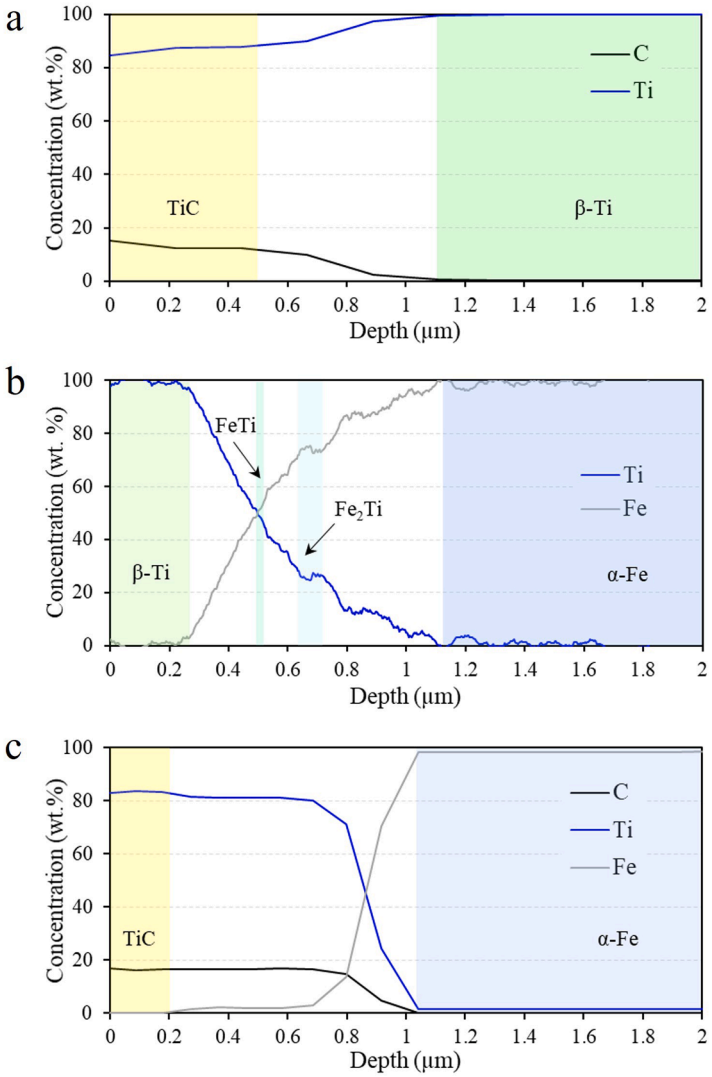

Fig. 3. (a) simulated C diffusion profiles after diffusion in 2 μm of Ti (model A) at 1000 °C for 10 min; (b) Experimental Fe and Ti EDX diffusion profiles at the film/substrate interface after sintering at 1050 °C for 10 min with graphite foil coated with 1.2 μm of Ti (model B); (c) C, Ti, and Fe simulated diffusion profiles after diffusion in 1 μm of TiC + 4 μm Fe at 1000 °C for 10 min (model C).

graphite foil-film interface up to 0.1 μm and with γ-Fe at greater depths. Since the carbon solubility in γ-Fe ranges from 0 to 2 wt. %, free carbon (*i.e.*, not combined with Ti to form TiC) can reach the iron substrate, causing the film to lose its protective behavior. Fig. 5 presents the carbon profiles and the phases present throughout the depth of the film and the sintered substrate for all five scenarios.

The influence of the film thickness can be understood from scenarios 1 (protective case) and 5 (unprotective case). With decreasing film thickness, the film/substrate interface progressively shifts toward the carbon side. Assuming the diffusion profiles (C in Ti from one side, and Fe in Ti from the other side) remain constant, the amount of iron coexisting with TiC increases. Disregarding the microstructure of the phases, if the iron concentration is low (*i.e.*, the film is sufficiently thick), α-Fe is stabilized and the substrate is protected due to TiC formation and the low C solubility in α-Fe. If the iron concentration is high (*i.e.*, the film is too thin), γ-Fe is stabilized, and the substrate loses its protection. This can be verified by shifting the iron diffusion profile from scenario 1 toward the carbon side while keeping the carbon profile unchanged and balancing with titanium: as a result, the system enters the γ domain. The amount of carbon dissolved into γ-Fe increases from 0 to 2 wt. % with decreasing film thickness, consistent with the experimental measurements (Fig. 2).

The approach used in the present study applied to the C-Ti-Fe system is based on the complementary integration of thermodynamic simulations and available experimental data, which complement each other. This approach successfully described a complex system where neither simulations nor experiments alone are sufficient. It can be extended to other film-substrate combinations to help quickly identify the most promising barriers against carbon diffusion during SPS and optimize their thickness, thereby reducing the number of experimental tests and associated costs. More broadly, these findings suggest an approach that could be applied in other environments where limiting carbon contamination is critical.

CRediT authorship contribution statement

R. Charvet: Writing – original draft, Validation, Investigation. **M.R. Ardigo-Besnard:** Writing – review & editing, Validation, Supervision, Project administration, Funding acquisition, Conceptualization. **A. Besnard:** Writing – review & editing, Validation, Supervision, Conceptualization. **F. Baras:** Writing – review & editing, Validation, Supervision, Conceptualization. **S. Le Gallet:** Writing – review & editing, Validation, Supervision, Conceptualization. **Y. Pinot:** Writing – review & editing, Validation, Supervision, Investigation, Conceptualization. **F.**

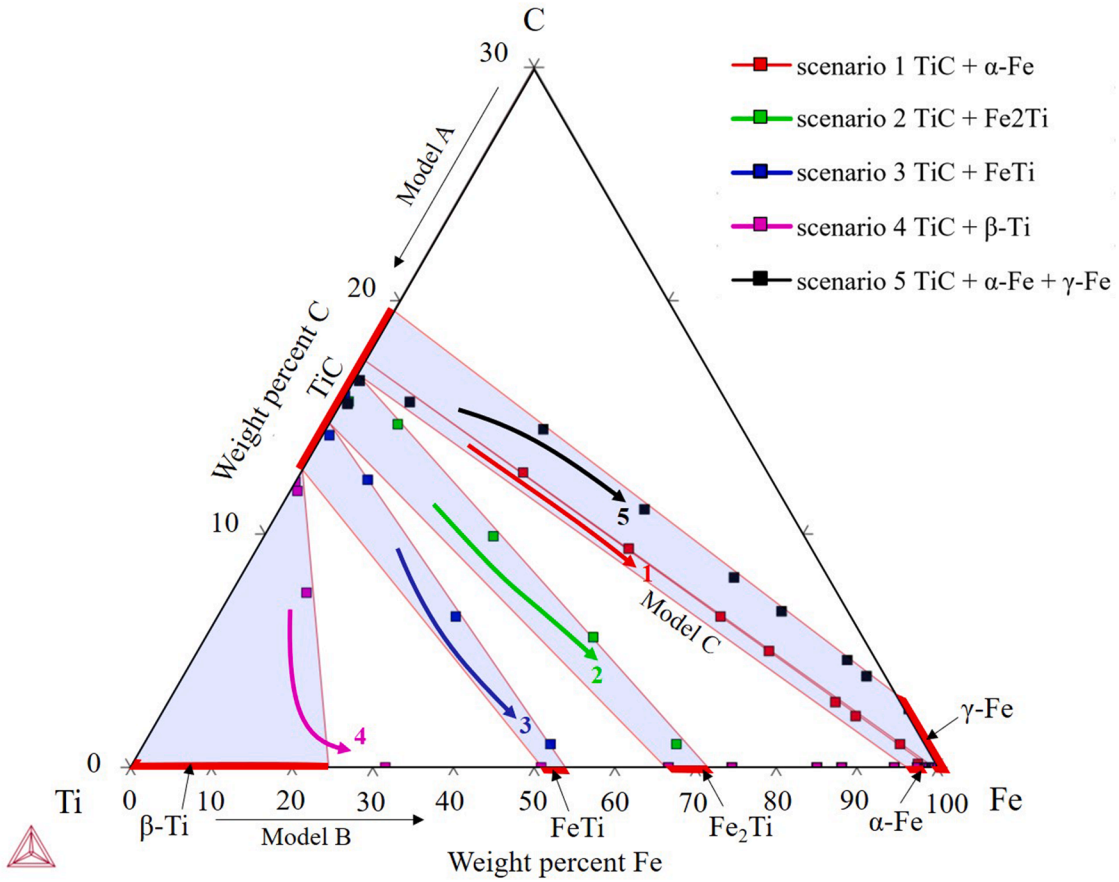

Fig. 4. C-Ti-Fe isopleth section at 1000 °C representing the scenarios obtained by plotting the elemental values of the models shown in Fig. 5.

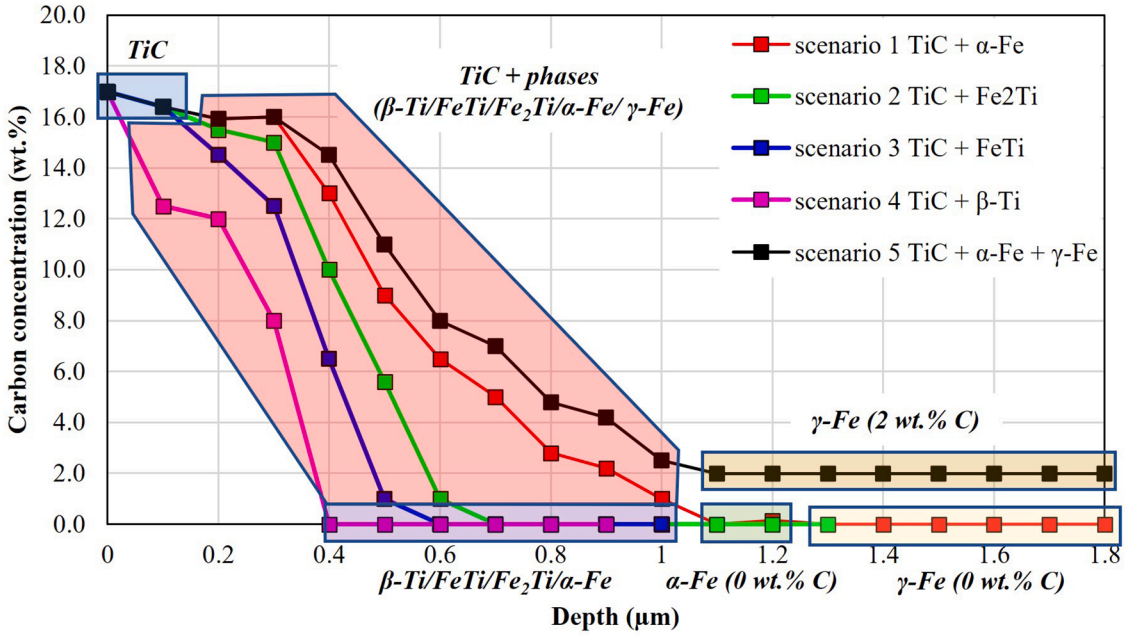

Fig. 5. Diffusion scenarios obtained by combining carbon simulation values and iron and titanium experimental profiles.

Herbst: Investigation. **F. Bernard:** Writing – review & editing, Validation, Supervision, Conceptualization.

Declaration of competing interest

The authors declare the following financial interests/personal relationships which may be considered as potential competing interests:

Maria-Rosa Ardigo-Besnard reports financial support was provided by French National Research Agency. Frederic Bernard reports equipment, drugs, or supplies was provided by French National Research Agency. If there are other authors, they declare that they have no known competing financial interests or personal relationships that could have appeared to influence the work reported in this paper.

Acknowledgements

This work was financed by the ANR PRCE OEDIPUS project (Grant ANR-23-CE08–0028) and was performed in the CALHIPSO/EQUIPEX+ platform (Grant ANR-21-ESRE-0039).

Supplementary materials

Supplementary material associated with this article can be found, in the online version, at doi:10.1016/j.scriptamat.2025.116983.

References

[1] M.R. Ardigo-Besnard, A. Tellier, A. Besnard, J.-P. Chateau-Cornu, Effect of the microstructure on the tribological properties of HIPed and PTA-welded Fe-based hardfacing alloy, Surf. Coat. Technol. 425 (2021) 127691, https://doi.org/10.1016/j.surfcoat.2021.127691.

[2] T. Voisin, J.-P. Monchoux, L. Durand, N. Karnatak, M. Thomas, A. Couret, An innovative way to produce γ-TiAl blades: spark plasma sintering, Adv. Eng. Mater 17 (2015) 1408–1413, https://doi.org/10.1002/adem.201500019.

[3] R. Mvodo Eba, M.R. Ardigo-Besnard, J.-P. Chateau-Cornu, F. Herbst, N. Geoffroy, A. Besnard, C. Vandenabeele, S. Lucas, A. Descamps-Mandine, C. Josse, Phase transformation mechanisms occurring during spark plasma sintering elaboration of new duplex composite stainless steels, Mater. Chem. Phys 325 (2024) 129796, https://doi.org/10.1016/j.matchemphys.2024.129796.

[4] P. Angerer, L.G. Yu, K.A. Khor, G. Krumpel, Spark-plasma-sintering (SPS) of nanostructured and submicron titanium oxide powders, Mater. Sci. Eng.:. A 381 (2004) 16–19, https://doi.org/10.1016/j.msea.2004.02.009.

[5] K. Zaara, M. Chemingui, S.Le Gallet, Y. Gaillard, L. Escoda, J. Saurina, J.J. Suñol, F. Bernard, M. Khitouni, V. Optasanu, High-entropy FeCoNiB0.5Si0.5 alloy synthesized by mechanical alloying and spark plasma sintering, Crystals 10 (2020) 929, https://doi.org/10.3390/cryst10100929.

[6] A. Bolsonella, F. Naimi, O. Heintz, T. Tricone, H. Couque, F. Bernard, Influence of oxygen induced during high-energy ball milling process on the mechanical properties of sintered nickel by SPS, J. Alloys. Compd 856 (2021) 157869, https://doi.org/10.1016/j.jallcom.2020.157869.

[7] C. Menapace, I. Lonardelli, A. Molinari, Phase transformation in a nanostructured M300 maraging steel obtained by SPS of mechanically alloyed powders, J. Therm. Anal. Calorim 101 (2010) 815–821, https://doi.org/10.1007/s10973-010-0745-5.

[8] K.E. Smetanina, P.V. Andreev, A.V. Nokhrin, E.A. Lantsev, V.N. Chuvildeev, Carbon contamination during spark plasma sintering of powder materials: a brief overview, J. Alloys. Compd 973 (2024) 172823, https://doi.org/10.1016/j.jallcom.2023.172823.

[9] N. Kwak, G. Min, Y. Oh, D.-W. Suh, H.C. Kim, S. Kang, H.N. Han, Tantalum and molybdenum barriers to prevent carbon diffusion in spark plasma sintered tungsten, Scr. Mater 196 (2021) 113759, https://doi.org/10.1016/j.scriptamat.2021.113759.

[10] M.-R. Ardigo-Besnard, A. Besnard, M. Moser, F. Bussière, Development of Ti PVD films to limit the carburization of metal powders during SPS process, Solids 2 (2021) 395–406, https://doi.org/10.3390/solids2040025.

[11] M. Evrard, A. Besnard, S. Lucas, Study of the influence of the pressure and rotational motion of 3D substrates processed by magnetron sputtering: a comparative study between Monte Carlo modelling and experiments, Surf. Coat. Technol. 378 (2019) 125070, https://doi.org/10.1016/j.surfcoat.2019.125070.

[12] X.L. Li, R. Hillel, F. Teyssandier, S.K. Choi, F.J.J. Van Loo, Reactions and phase relations in the TiAlO system, Acta. Metall. Mater. 40 (1992) 3149–3157, https://doi.org/10.1016/0956-7151(92)90478-W.

[13] J.-M. Auger, D. Cotton, C. Nouveau, A. Besnard, F. Bernard, M.-R. Ardigo-Besnard, J.-P. Monchoux, R. Cours, C. Marcelot, Comparison of thermal diffusion and interfacial reactions for bulk and sputtered titanium on 316L stainless steel, Mater. Chem. Phys 306 (2023) 128013, https://doi.org/10.1016/j.matchemphys.2023.128013.